Removal of NO at low concentration from air in urban built environments by activated miscanthus biochar

Journal of Environmental Management 336 (2023) 117610

Contents lists available at ScienceDirect

Journal of Environmental Management

journal homepage: www.elsevier.com/locate/jenvman

Research article

Removal of NO at low concentration from air in urban built environments by activated miscanthus biochar

Carlos G. Díaz-Maroto [a,b], Blanca Sáenz de Miera [a], Laura Collado [b,c], Jose Fermoso [d], Ondřej Mašek [e], Patricia Pizarro [a,b], David P. Serrano [a,b], Inés Moreno [a,b], Javier Fermoso [a,*]

[a] Thermochemical Processes Unit, IMDEA Energy, Avda. Ramón de La Sagra 3, 28935, Móstoles, Madrid, Spain
[b] Chemical and Environmental Engineering Group, Rey Juan Carlos University, Móstoles, Madrid, Spain
[c] Photoactivated Processes Unit, IMDEA Energy, Avda. Ramón de La Sagra 3, 28935, Móstoles, Madrid, Spain
[d] Natural Resources and Climate Area, CARTIF Technology Centre, Parque Tecnológico de Boecillo, 205, 47151, Valladolid, Spain
[e] UK Biochar Research Centre, School of Geosciences, University of Edinburgh, Crew Building, Alexander Crum Brown Road, Edinburgh, EH9 3FF, UK

ARTICLE INFO

Keywords:
Activated biochar
Polluted air
NOx removal
NO oxidation
Carbon catalysts
Low concentration NO

ABSTRACT

This work presents an innovative and sustainable approach to remove NO emissions from urban ambient air in confined areas (underground parking areas or tunnels) using low-cost activated carbons obtained from Miscanthus biochar (MSP700) by physical activation (with CO_2 or steam) at temperatures ranging from 800 to 900 °C. The NO removal capacity of the activated biochars was evaluated under different conditions (temperature, humidity and oxygen concentration) and compared against a commercial activated carbon. This last material showed a clear dependence on oxygen concentration and temperature, exhibiting a maximum capacity of 72.6% in air at 20 °C, whilst, its capacity notably decreased at higher temperatures, revealing that physical NO adsorption is the limiting step for the commercial sample that presents limited oxygen surface functionalities. In contrast, MSP700-activated biochars reached nearly complete NO removal (99.9%) at all tested temperatures in air ambient. Those MSP700-derived carbons only required low oxygen concentration (4 vol%) in the gas stream to achieve the full NO removal at 20 °C. Moreover, they also showed an excellent performance in the presence of H_2O, reaching NO removal higher than 96%. This remarkable activity results from the abundance of basic oxygenated surface groups, which act as active sites for NO/O_2 adsorption, along with the presence of a homogeneous microporosity of 6 Å, which enables intimate contact between NO and O_2. These features promote the oxidation of NO to NO_2, which is further retained over the carbon surface. Therefore, the activated biochars studied here could be considered promising materials for the efficient removal of NO at low concentrations from air at moderate temperatures, thus closely approaching real-life conditions in confined spaces.

1. Introduction

Air pollution in urban areas is recognized as a major public health problem ((WHO), n.d.; Derwent and Hjellbrekke, 2019). Among the main air pollutants, nitrogen oxides (NOx), produced by combustion engines and other combustion sources, are of particular concern due to their negative health issues (respiratory diseases) and environmental impacts (photochemical smog, acid rain, greenhouse effects and, stratospheric ozone depletion) (Yadav and Prasad, 2016). Road transport is still the most important source of NOx emissions in the EU-27, representing 39% in 2017 (Degrauewe et al., 2019; Derwent and Hjellbrekke, 2019). NOx are constituted by 95% NO, 4.5% NO_2 and the rest of N_2O (Yadav and Prasad, 2016).

Several methods have been developed for the removal of NOx, such as NSR (NOx Storage Reduction), SNCR (selective non-catalytic reduction), and Selective Catalytic Reduction (SCR) (Belala et al., 2014; Jeguirim et al., 2018; Zhao et al., 2016a). However, they face several limitations such as high cost, low efficiency, complexity, and narrow reaction conditions. In particular, SCR is the most commonly used method for NOx abatement in exhaust gases. However, this process presents some drawbacks, such as high reaction temperature (>300 °C) and leakage of ammonia or un-reacted reducing agents (Muñiz et al., 1999; Shen et al., 2016), which make it not suitable for the removal of NO emissions at low concentrations and under conditions typically

* Corresponding author.
E-mail address: javier.fermoso@imdea.org (J. Fermoso).

https://doi.org/10.1016/j.jenvman.2023.117610
Received 2 January 2023; Received in revised form 22 February 2023; Accepted 25 February 2023
Available online 2 March 2023

found in parking lots and tunnels (relatively low temperatures and high oxygen concentration) (Deng et al., 2020; Wang et al., 2015).

NO oxidation to NO_2 is being studied as an alternative NOx abatement strategy (Ghouma et al., 2018; Jeguirim et al., 2018; Shen et al., 2016; You et al., 2017). This process can proceed at room temperature and the generated NO_2 can be subsequently captured in water. Different types of materials such as zeolites (Labaki et al., 2010), perovskites (Hodjati et al., 2000), metal-supported oxides (Levasseur et al., 2011), and carbons (Deng et al., 2020; Jeguirim et al., 2018; Sousa et al., 2011; Zhang et al., 2008), etc. have been evaluated as catalysts for this reaction. Among them, carbon-based materials (active carbons, carbon fibres, carbons xerogels, etc.) are considered the most promising catalysts for NO oxidation as they offer many advantages such as high efficiency at room temperature and low energy requirements (Jeguirim et al., 2018; Shen et al., 2016; Sousa et al., 2011, 2012, 2013; Zhang et al., 2008; Zhu et al., 2022). However, despite the potential of carbon materials for the abatement of NOx emissions, the reaction mechanism and the parameters that govern this process are still debated (Deng et al., 2020; Shen et al., 2016). In their work, Zhang et al. suggested that NO oxidation is favored by the presence of narrow micropores, being independent of the surface area. The authors proposed that NO and O_2 are co-adsorbed in the carbon micropores, yielding NO_2, with no significant impact of the carbon chemical properties (Zhang et al., 2008). According to the recent work reported by Zhu et al. (2022), the microporous surface area and degree of hierarchy are key factors affecting NO conversion due to the enhanced diffusion of the reactants. However, other researchers reported that NO removal efficiency can be promoted by changing the composition and distribution of surface functional groups, which act as adsorption sites (Adapa et al., 2006; Mochida et al., 1997). Rathore et al. proposed that both NO and O_2 are adsorbed on the functionalized sites of activated carbon, over which the NO oxidation into NO_2 occurs. Then, the adsorbed NO_2 further reacts and forms various intermediates in the adsorbed phase, such as NO_3 and NO–NO_3, the latter being finally desorbed in the form of NO_2 (Rathore et al., 2010). Most studies reported in the literature have been carried out using high NOx concentrations (450–1000 ppm), simulating combustion flue gases in the presence of oxygen and evaluating the catalytic behaviour of the carbonaceous solid once the steady state was reached. On the contrary, there are just rare works investigating the NOx removal at very low concentration (5 ppm NO_2) by activated carbons, such as that of Ghouma et al. (2017). However, to our knowledge, no previous works have directly dealt with the treatment of polluted air with low NO concentration (<20 ppm). Here, this work focuses on the removal of NO at similar concentrations to those found in built environment and transport infrastructure (i.e, less than 5 ppm), using low-cost carbon materials obtained from biomass residues.

Biochar is the solid fraction obtained by pyrolysis of biomass. It has been widely used in environmental applications (Cha et al., 2016; Wang and Wang, 2019), such as soils amendment, carbon sequestration, and water treatment (e.g. metal-contaminated) (Li et al., 2017); or as a fuel in energy production for the pyrolysis process itself (Jafri et al., 2018). There are other applications such as catalyst support or catalyst itself, pollutants adsorbent (in gas or aqueous phase) and energy storage (Liu et al., 2015). Biochar is carbon-rich, exhibits a porous structure, and maintains certain surface functional groups and mineral components of the raw biomass, properties that favor its use as active carbon precursor (Tan et al., 2017). To improve their porous structure, surface area, and surface chemistry, different activation methods have been widely used, based on both physical, using CO_2, diluted O_2 or steam at high temperatures (600–1200 °C), and chemical treatments by impregnation with a chemical reagent such as KOH, H_3PO_4, $ZnCl_2$, etc., followed by a carbonization at 400–900 °C (Ahmed et al., 2016). More recently, new activation methods such as fine-tuned micropore biochar by lignin impregnation (Zhang et al., 2022), and ball milling with hydrogen peroxide or ammonia hydroxide (Qi et al., 2022) have been successfully developed and applied for the preparation of active carbons from pyrolysis biochars.

In the case of the physical activation, the biochar is partially oxidized at high temperatures leading to an activated carbon with an accessible and well-developed porous structure (Chang et al., 2000; Yang and Lua, 2003). In this regard, the nature of the raw biochar, the gasifying agent employed as well as the activation time and temperature will determine the final properties (surface chemistry, porosity, etc.) of the resultant carbonaceous solid (Chang et al., 2000; Ghouma et al., 2017; Jeguirim et al., 2018; Nowicki et al., 2010).

To reduce costs and use more sustainable raw materials for the active carbon preparation, in this work we propose the activation of biochar obtained as by-product of the pyrolysis of lignocellulosic biomass, specifically *Miscanthus giganteus*. Miscanthus is a promising energy crop with high potential to produce biofuels and/or biochemical precursors, as it is fast-growing, does not compete with food production, and can be developed sustainably with efficient use of water (Delmotte et al., 2015; Mimmo et al., 2014).

Therefore, the idea behind this study was to investigate for the first time in the literature the removal of NO at low concentration (<5 ppm) from polluted air with physically activated carbons (CO_2 and H_2O) derived from the pyrolysis biochar of Miscanthus straw pellets, as a low-cost and environmentally friendly carbonaceous precursor. At room temperature and under dry air flow, the results here reported demonstrate that these activated biochars show almost full NO removal efficiency, being much higher than those exhibited by a commercial carbon of mineral origin (740GR). These results denoted the huge potential of these materials to be installed in filters located in confined or semi-closed spaces, like underground parking lots and road tunnels, which are characterized by distinct ambient conditions. Although, at this stage of the investigation, a cost-study of the process has not been done yet, it will be considered for future works. To develop a better understanding of the NO removal mechanism from low-concentration gas streams, three important operation variables were evaluated in this work: oxygen concentration, relative humidity and temperature.

2. Materials and methods

2.1. Materials

In this work, the performance of different low-cost and renewable activated carbons, derived from the activation of biochar, in NOx removal has been investigated and compared with that of one commercial active carbon of mineral origin and activated with steam at 900 °C (740GR) acquired from Chiemivall, S.L.

Miscanthus straw, in form of pellets (MSP) with an average particle size of 10 mm length and 5 mm diameter, was used as raw material for biochar production. MSP sample was pyrolyzed in a rotary kiln reactor. The reaction conditions were established at a temperature of 700 °C, a heating rate of 80 °C/min and a residence time of 12 min, giving rise to the MSP700 biochar with a mass yield of 21 wt.% (Mašek et al., 2018). MSP700 was then used as a carbonaceous precursor to produce the activated biochars by means of physical activation.

2.2. Biochar activation

2.2.1. Physical activation: CO_2 and steam

MSP700 biochar was physically activated with either CO_2 or steam in a lab-scale reactor, whose description, schematic diagram (displayed in Fig. S1) and a detailed experimental procedure are provided in the Supplementary Material.

For both activation processes the degree of activation or burn-off level of the obtained carbonaceous materials is an important parameter that can be calculated from the following equation:

$$burn-off\ (wt.\%) = \frac{W_{0,daf} - W_{f,daf}}{W_{0,daf}} \bullet 100 \qquad \text{Equation 1}$$

Where $W_{0,daf}$ and $W_{f,daf}$ are the weight of biochar (in dry and ash free basis) before and after the activation process, respectively.

2.3. Physico-chemical characterisation of samples

Proximate analysis of MSP, biochar (MSP700) and activated biochars were performed according to European standards. Ultimate analysis of carbonaceous samples was measured in a Thermo Scientific FLASH 2000 CHNS/O micro-elemental analyzer, where C, H and N concentrations were obtained, while O concentration was calculated by difference. The morphology of the activated carbon particles was observed by means of Field Emission Scanning Electron Microscopy (FE-SEM) in a JEOL JSM-7900 F microscope operating at 1 Kv. Activated carbons were subjected to N_2 and CO_2 adsorption-desorption analyses at 77 K and 273 K, respectively, in a Micromeritics 3Flex instrument. The point of zero charge (pH_{PZC}), defined as the pH at which the net charge of total sample surface is equal to zero, was also determined. X-ray photoelectron spectra (XPS) were recorded with a PHOIBOS 100 hemispherical electron energy analyzer (SPECS) and CasaXPS was employed for data collection and interpretation. Temperature Programmed Desorption (TPD) measurements were carried out using an AUTOCHEM II 2910 instrument (Micromeritics), equipped with a thermal conductivity detector (TCD) and coupled to a quadrupole mass spectrometer (MS) Pfeiffer Omnistar GSD350. All of these physico-chemical characterisation techniques and the corresponding experimental procedures have been described in the Supplementary Material.

2.4. NO removal tests from polluted gaseous streams

A lab-scale filter, whose schematic diagram can be seen in Fig. 1, has been employed for the NO removal tests from gaseous streams.

This setup consists of a glass updraft fixed-bed column (500 mm length, 16 mm i.d.) with a porous plate, in which 3 g of activated carbon is placed. The filter-column is externally covered by a heating tape in the area where the carbon material is located to control and evaluate the temperature effect of the NO removal tests (20–75 °C). This filter possesses a gas inlet coming from a valves system, which is used to generate different contaminated gaseous streams; and a gas outlet that is conducted to the NO_x analyzer (Ecotech Serinus 40) prior to being delivered to vent. The generation system of polluted gaseous streams consists of three gas cylinders: N_2 (99.999 vol%), synthetic air (99.999 vol%), and 50 ppm NO (balance N_2), which are fed from independent mass flow controllers (MFCs) to set the concentration of NO and O_2 in the gas stream with a total flow rate of 1000 NmL/min. Firstly, the polluted gas current is generated by diluting NO flow in an air/N_2 stream (dry or with a certain relative humidity) in a gas mixer, in which there is a probe that allows the continuous monitorization of the temperature and relative humidity of the gas stream. To produce humid air stream, a controlled share of the air flow was passed through a flask containing Milli-Q water at room temperature before being mixed with the NO flow (see Fig. 1). Finally, the generated low concentration NO gas stream (5 ppm NO) is alternatively directed to the filter column to perform the NO_x removal tests or by-passed to the gas analyzer (to check the composition of the initial air stream).

In this work, the performance of the activated biochars on NO removal was evaluated for 400 min by investigating both, the effect of the activation conditions: temperature (800–900 °C) and activating agent (CO_2 or steam); but also, the effect of three important operation parameters such as: the effect of the O_2 concentration (0, 4, 15 and 21 vol%), the adsorption temperature (20, 50 and 75 °C) and the presence of relative humidity (0 and 50 vol% RH) in the air stream.

First, blank tests were performed in absence of any solid sample. For that purpose, N_2 and air flow were used to evaluate if the oxidation of NO to NO_2 could take place in the gas phase under oxidizing atmospheres in absence of carbon. No evidence of such oxidation was found, obtaining invariable NO and negligible NO_2 concentrations at the outlet of the reactor, which agrees with previous works reported in the literature (Tsukahara et al., 1999; Zhu et al., 2000). Moreover, to discard the catalytic activity of the inorganic matter contained in the MSP-derived carbons, an additional experiment was performed using an ashes-bed, obtained by the combustion of the raw MSP700 biochar. In this assay, the NO elimination was almost null, denoting that the inorganic matter contained in the physically activated biochars do not contribute to their NO removal ability.

The NO elimination capacity was calculated according to the following equation:

$$NO_{elimination}(\%) = \frac{NO_{in}(mg) - NO_{out}(mg)}{NO_{in}(mg)} \bullet 100 \qquad \text{Equation 2}$$

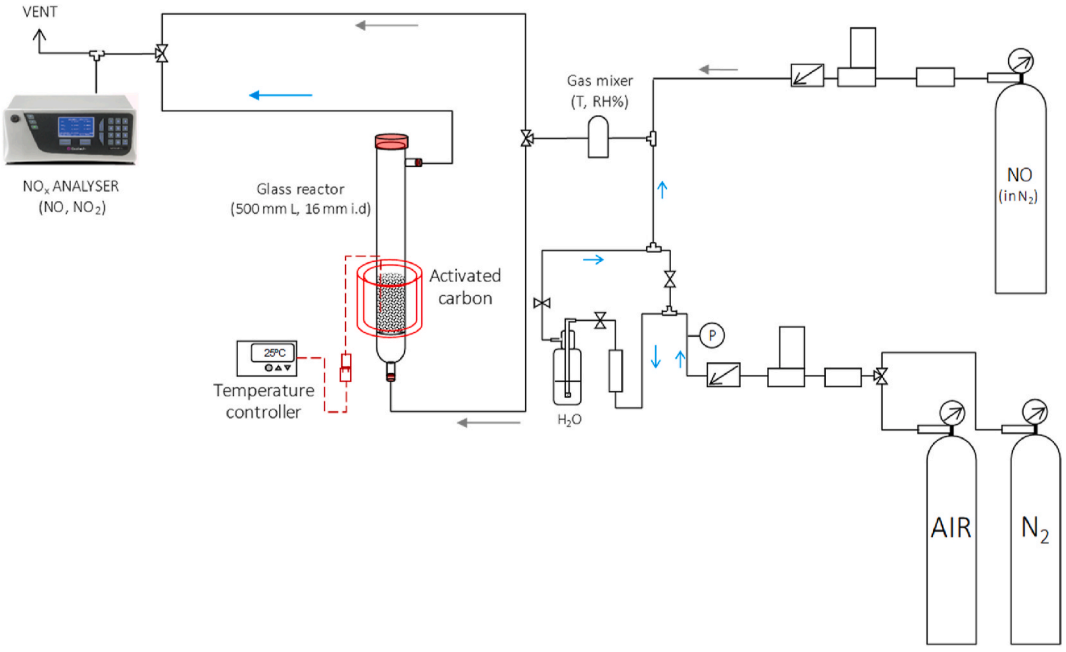

Fig. 1. Schematic diagram of the lab-scale filter to remove NO_x (NO and NO_2) from contaminated gaseous streams.

Where, NO_{in} and NO_{out} represent the total amount of NO (in mg) fed and remaining in the exhaust gas, respectively.

Most of the research works devoted to NOx abatement from flue gases accept that NO removal involves NO oxidation to NO_2 (Mochida et al., 2000; Rathore et al., 2010; Sousa et al., 2011; Zhang et al., 2014b), which can be further released and retained in water as nitric acid (Sousa et al., 2011). However, during the experiments here performed, the NO_2 concentration at the outlet of the adsorption system remained almost invariable at negligible values. Therefore, this work mainly focuses its attention on the adsorption breakthrough curves (plotting C/C_0 of NO versus time) and the total NO removal capacity of the investigated materials for 400 min of the test.

3. Results and discussion

3.1. Physico-chemical characterization of activated carbon materials

Proximate and ultimate analyses of the raw MSP, MSP700 biochar, the corresponding materials obtained by physical activation, and the commercial activated carbon (740GR) are shown in Table 1, also including the degree of activation (burn-off) obtained by the different activation methods applied.

The proximate analysis shows that the pyrolysis process led to the loss of most of the volatiles contained in the raw MSP. This, in turn, resulted in a significantly higher ash share since the inorganic matter present in the pyrolysis biochar is hardly affected by the thermal treatment. Accordingly, the fixed carbon content was substantially raised due to the removal of the volatile matter. As revealed by the ultimate analysis (dry ash free basis), a significant enrichment in carbon content takes place to the detriment of oxygen and hydrogen. This finding is somehow observable in the van Krevelen diagram (Fig. 2), in which MSP700 is significantly shifted to a lower-left position due to the decrease in the H/C and O/C atomic ratios in comparison with the MSP parent sample. This behavior indicates that the biochar is deeply carbonized and exhibits a highly aromatic structure (Chen et al., 2008; Chun et al., 2004; Keiluweit et al., 2010), which is modified after the activation leading to a further reduction of the O/C and especially H/C ratios, getting closer to the commercial activated carbon 740GR (Hwang et al., 2017).

Activation with CO_2 is an oxidative treatment that eliminates C atoms from the biochar through a heterogeneous endothermic reaction that releases gaseous CO. The activation of MSP700 with CO_2 at the lowest temperature (800 °C) leads to a slightly higher oxygen content than the parent biochar, as shown in the van Krevelen diagram (Fig. 2), which can be ascribed to the chemisorption of some oxygen on the carbon surface during the gasification reaction, forming C(O) surface complexes (Chen et al., 2017; Fritz and Ttinger, 1993). This effect seems to be attenuated at higher activation temperatures, leading to lower O/C ratios on the Van Krevelen graph, which can be attributed to the higher burn-off level, from 19.2 to 34.4 wt.%, as expected considering that CO_2 gasification is an endothermic process favored by temperature. Consequently, the remaining volatile matter of the MSP700 biochar was completely removed at any activation temperature, while the ash content continued progressively growing with the activation process, due to the decrease of the fixed carbon.

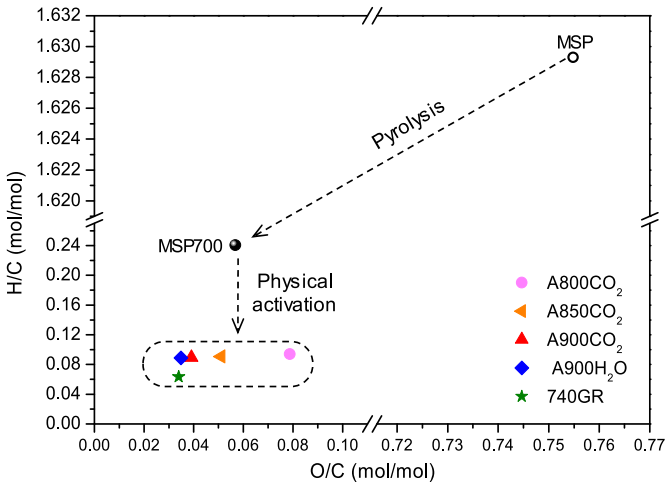

Fig. 2. Van Krevelen diagram showing the H/C against O/C (dry ash free basis) for the MSP, MSP700, and activated derived biochars and commercial 740GR activated carbon.

The physical activation of MSP700 at 900 °C with CO_2 ($A900CO_2$) and steam ($A900H_2O$) gave rise to very similar burn-off percentages (≈34 wt.%), ash content and fixed carbon. It denotes that steam is a more reactive gasifying agent than CO_2, due to the activating time was 60 and 90 min, respectively, which is in accordance with the literature (González et al., 2009; Román et al., 2008; Sajjadi et al., 2019).

In summary, from the van Krevelen diagram, it can be concluded that MSP700 activated biochars present a more condensed aromatic structure than the biochar precursor (Qu et al., 2021). No large differences were observed between the activated biochars, in terms of elemental analysis (dry ash free basis), in comparison to the commercial active carbon, with the exception of $A800CO_2$ that presented rather larger oxygen content due to the relatively low activation temperature.

Fig. S2 shows the SEM micrographs of raw MSP700 biochar (A), MSP700-derived CO_2 (B) and steam (C) activated carbons, as well as those for the commercial carbon 740GR (D). In Figures S2 (B) and (C) can be appreciated at first sight the development of a new open porosity, in the range of mesopores, on MSP700-derived carbons after being exposed to physical activation, which does not appear in the raw biochar neither in the commercial carbon.

N_2 and CO_2 adsorption-desorption isotherms for MSP700, activated biochars and 740GR are shown in Fig. S3 A) and B), respectively. Raw MSP700, as expected with this kind of materials (biochar) obtained from lignocellulose pyrolysis, shows a small surface area because its porosity has not been well developed yet as shown in SEM images. It presents a limited and very narrow microporosity, in which, the access of N_2 molecules may be restricted because of the extremely slow diffusion of N_2 into the ultramicropores at 77 K may significantly delay or restrict

Table 1
Proximate and ultimate analysis of MSP, MSP700 biochar and derived activated biochars in comparison with commercial activated carbon (740GR).

Sample	Burn-off (wt.%)	Proximate Analysis, db (wt.%)			Ultimate Analysis, daf (wt.%)				
		Volatile Matter	Ash	Fixed Carbon	C	H	N	S	O
MSP	–	70.4	3.9	25.7	46.4	6.3	0.6	0.0	46.7
MSP700	–	9.7	18.8	70.0	89.8	1.8	1.6	0.0	6.8
$A800CO_2$	19.2	0.0	24.7	75.3	89.5	0.7	0.3	0.0	9.4
$A850CO_2$	29.7	0.0	27.3	72.7	92.6	0.7	0.4	0.0	6.3
$A900CO_2$	34.4	0.0	28.7	71.3	93.9	0.7	0.5	0.0	4.9
$A900H_2O$	33.9	0.0	28.6	71.4	94.6	0.7	0.3	0.0	4.4
740GR	–	0.0	9.5	90.5	94.8	0.5	0.2	0.2	4.3

db: dry basis; daf: dry and ash free basis.

equilibration during adsorption process at low pressures (Garrido et al., 1987; Jagiello et al., 2019).

In the case of MSP700 activated biochars, the shape of N_2 isotherms at low relative pressures corresponds to type I(a), assigned to microporous materials with a homogeneous pore size (Thommes et al., 2015). These isotherms present a relatively narrow H4 hysteresis loop (according to the IUPAC classification) in the range of low-medium pressures, which is often assigned to the presence of narrow slit micropores. This hysteresis loop becomes wider in the biochars subjected to a physical activation (CO_2 and steam) at high temperatures (850–900 °C) which could denote the formation of larger micropores. On the other hand, the commercial activated carbon (740GR) presents a type I (b) isotherm, characteristic of materials with a relatively broad pore size distribution, including larger micropores and possibly small mesopores (Thommes et al., 2015). This material exhibits a higher adsorption capacity in comparison with the activated biochars and, therefore, much higher values of the textural parameters (see Table 2). Thus, the commercial sample show S_{BET} and S_{MICRO} of 818 and 751 m^2/g, respectively, while the activated biochars are ranged from 462 to 562 m^2/g and 418–502 m^2/g. Likewise, the micropore volume is much higher in 740GR (0.342 cm^3/g) than in activated biochars (0.192–0.230 cm^3/g). In the case of CO_2 activated biochars, the textural parameters increase with the activation temperature. This fact is related to the higher degree of burn-off achieved during the activation of the biochar at higher temperatures. In contrast, the activated biochar with steam exhibit lower values of S_{BET}, S_{MIC} as well as V_{TOTAL} and V_{MIC} than that activated with CO_2, suggesting that the activation temperature has a more significant impact than the activation agent on the development of textural properties of this carbonaceous precursor.

The pore size distribution of the raw MSP700, activated biochar samples and the commercial carbon was determined through the combination of both CO_2 and N_2 isotherms, by applying the model 2D-NLDFT and considering a slit pore geometry (Fig. 3). For clarity, the CO_2 isotherm is used to define the ultra-small microporosity zone (pore size <10 Å), while the N_2 isotherm allows the estimation of the pore size distribution in the large-microporous and mesoporous range (pore size >10 Å) (Jagiello et al., 2019). As it can be observed, the commercial activated carbon (740GR) shows a broad and overlapping pore size distribution in the micropore (with pore diameters of 6.3 and 11 Å) and small mesopores range, in accordance with the shape of the N_2 isotherm previously discussed. In contrast, the physically activated biochars exhibit a homogeneous microporosity centred at ~5.8–5.9 Å. Despite the lower specific surface area of the MSP700 activated biochars compared to the commercial 740GR sample, the formation of a homogeneous porosity around 6 Å during the MSP700 biochars activation is an important feature, as this value seems to be optimal for the NO removal (Wang et al., 2011; Zhang et al., 2008). Additionally, in the case of the biochars activated with steam and CO_2 at 800−900 °C, a small proportion of small mesopores (36–37 Å) are also present, which can be related to the widening in the hysteresis loop observed in the isotherms corresponding to these materials (Fig. S3 A). This mesoporosity could also contribute to the NO catalytic oxidation (Zhu et al., 2022).

The elemental analysis was the primary method to identify and quantify the chemical composition of the samples; however, they do not provide any information about the functional groups present on the carbon surface.

The characterization of the different types of oxygen-containing functional groups is important since they may confer the surface with weak acidity, alkalinity, oxidative and reducing power, among other properties (Jeguirim et al., 2018). These diverse characteristics lead to activated carbons with varied surface chemistry and active sites, which may influence the binding ability of these materials with adsorbates, thus influencing the overall performance of the activated carbons. In this sense, the main surface functional groups of MSP700 activated biochars and commercial 740GR activated carbon were characterized with X-ray photoelectron spectroscopy (XPS) and temperature-programmed desorption coupled with a mass spectrometer (TPD-MS).

The high resolution C1s XPS spectra of activated biochars, A900CO_2 and A900H_2O, and the commercial carbon are depicted in Fig. 4A.

A broad peak assigned to carbon atoms mostly in graphite-like sp^2 (C_{sp2}, 284.7 eV) and sp^3 hybridization states (C–C, 285.6 eV) is present in the spectra of the three samples. The energy peak at 290.4 eV can be attributed to π-π* shake-up transitions in aromatic rings. Additional high-energy signals corresponding to carbon atoms bonded with hydroxyl or ether groups (C–OH or C–O–C, 286.3 eV); carbon in carbonyl groups, quinones and ketones (C═O, 287.4 eV); and carbon in carboxyl or ester groups (O–C═O, 289.3 eV) are also observed (Barroso-Bogeat et al., 2019; Haerle et al., 2002; Sysoev et al., 2018; Zhang et al., 2014a). The intensity of these signals is slightly higher in the MSP700-derived samples (see Table S1). Thus, the MSP700 activated biochars show lower sp^2/sp^3 area ratios (sp^2/sp^3 = 6.0 for A900CO_2 and 7.4 for A900H_2O activation, see Table S1) in comparison with the commercial carbon (sp^2/sp^3 = 11.8), which can be assigned to the presence of a higher proportion of defects or surface disorders (Jiang et al., 2013), suggesting a higher content of oxygen-containing functional groups on MSP700 activated biochars.

The O1s spectra (Fig. 4C) were deconvoluted into four peaks: oxygen doubly bonded to carbon in carbonyl groups and quinones (C═O, 531.5 eV), oxygen from hydroxyls and singly bonded to carbon in phenols, ethers and esters (O–H or C–O, 533.2 eV), oxygen doubly bonded to carbon from carboxyl groups or esters (-COOH or –COOR, 535.0 eV), and adsorbed H_2O and/or O_2 (ca. 536.9 eV) (Barroso-Bogeat et al., 2019; Huang et al., 2017; Pevida et al., 2008). C–O and hydroxyl groups are found predominant in all samples (Table S2), according to the higher content of C–OH groups found in XPS C1s spectra (Table S1), showing a relative higher proportion in the MSP700 activated biochars than in 740GR. In contrast, the proportion of oxygen bonded in carbonyl groups and carboxyl groups or esters (-COOH, –COOR) is also significant in the three carbons, with percentages ranging from 27 to 29% and 8–10%, respectively. The O1s/C1s atomic ratios, determined from C1s and O1s XPS survey spectra in MSP700 biochar is 0.18. This value is higher than that of activated biochars (ca. 0.13 and 0.10 for A900H_2O and A900CO_2, respectively), and that of 740GR (ca. 0.06). This finding further indicates a decrease in the total amount of oxygenated groups on the carbon surface during physical activation of MSP700, but still evidencing a higher amount of surface oxygenated functionalities in the activated MSP700 biochars than in the commercial carbon.

The TPD-MS method is adequate for the characterisation of oxygen functional groups on carbon with small porosity (Figueiredo and Pereira, 2010; Ishii and Kyotani, 2016). Therefore, TPD-MS analyses of activated biochars and commercial active carbon were performed to envisage the presence of different types of oxygenated functional groups. In this technique, the surface oxygen-containing groups on carbon materials are decomposed upon heating by releasing CO, CO_2 and H_2O and the nature of the oxygenated surface groups is related to the decomposition temperature and type of gas released. Fig. 5 shows the evolved profiles of H_2O, CO_2 and CO versus temperature obtained for the MSP700-activated biochars, A900CO_2 and A900H_2O, and the commercial sample (740GR), together with the temperature intervals

Table 2
Textural properties of the raw MSP700, activated biochars and the commercial carbon 740GR.

Sample	S_{BET} (m^2/g)	S_{MIC} (m^2/g)	V_{MIC} (cm^3/g)	V_{Total} (cm^3/g)
MSP700	63	n/a	n/a	n/a
A800CO_2	462	418	0.192	0.243
A850CO_2	513	459	0.220	0.291
A900CO_2	562	502	0.230	0.316
A900H_2O	542	469	0.219	0.299
740GR	818	751	0.342	0.400

S_{BET}: BET surface area; S_{MIC}: micropore surface area and V_{MIC}: micropore volume calculated using t-plot method; V_{Total}: total pore volume at $P/P_0 \approx 0.97$.

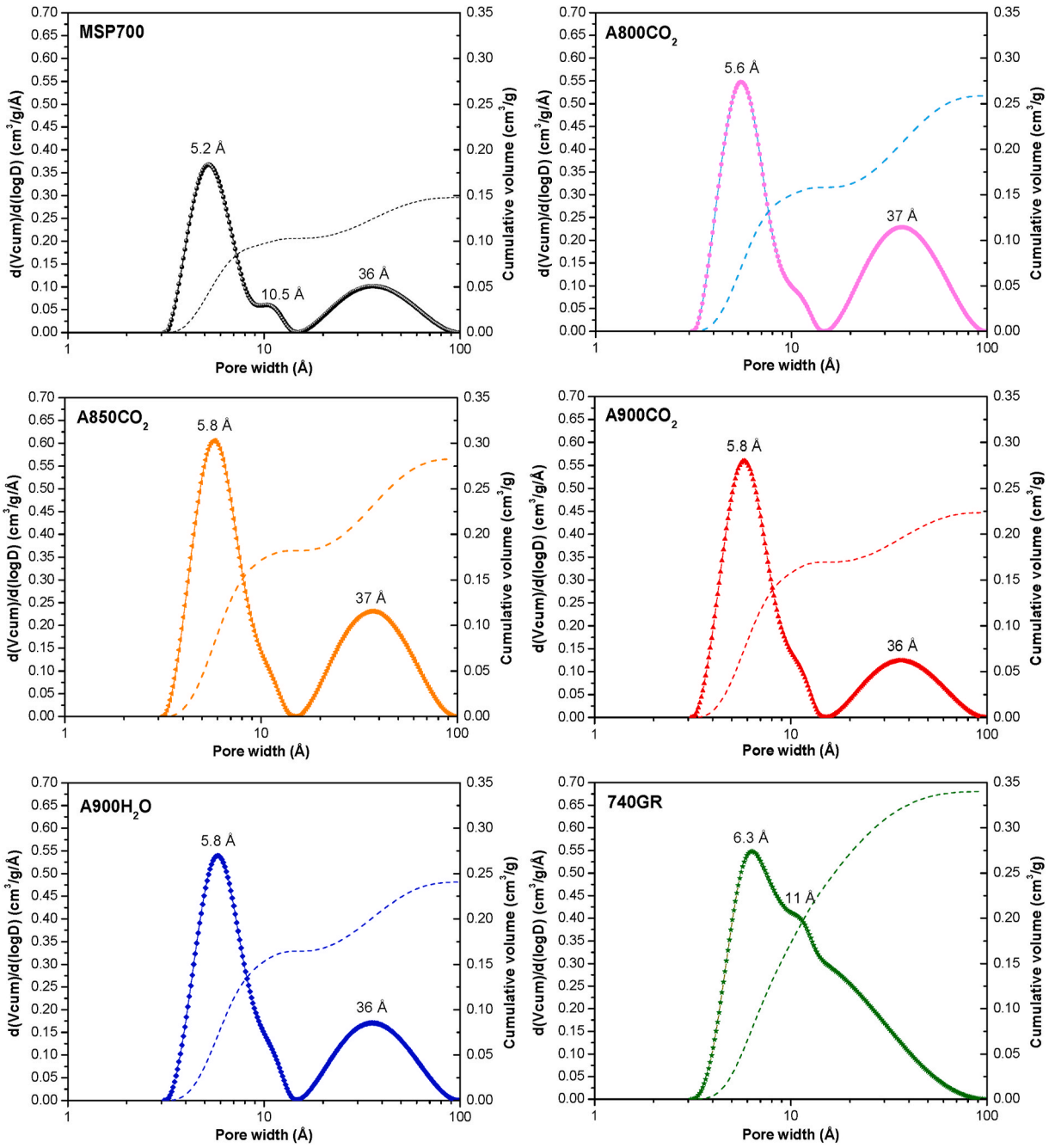

Fig. 3. 2D-NLDFT pore size distributions of MSP700 biochar, MSP700-derived carbons (activated with CO_2 and H_2O) and commercial activated carbon (740GR).

for the thermal decomposition of main surface oxygenated groups. As observed, both MSP700 activated biochars show relatively similar gases evolution profiles.

In the H_2O profile (Fig. 5A), the activated carbons derived from MSP700 biochar desorbed much more water than the commercial one. They display a composed desorption peak with two maximum centred at 200–210 °C and 350–370 °C, the latter being attributed to the presence of chemisorbed water that would be released due to dehydration reactions of neighbour hydroxyl groups, leading to the formation of carboxylic anhydrides, which further decompose at higher temperature to CO and CO_2 (350–627 °C) (Ghouma et al., 2015; Otake and Jenkins, 1993; Shafeeyan et al., 2010).

Regarding CO_2 desorption (Fig. 5B), this is specific to strong acidic groups and, in this case it exhibits a broad desorption band with a shoulder centred at 200–215 °C, along with a maximum peak centred at 320–340 °C, which could be associated to the presence of carboxylic and lactone groups (Figueiredo et al., 1999; Shafeeyan et al., 2010; Shen et al., 2012). There is also a CO_2 desorption signal at higher temperatures (560–575 °C), in particular in the case of A900CO_2 sample, which could be related to the carboxylic anhydride decomposition, as it overlaps with the starting of the CO desorption profile (Fig. 5C) (Ghouma et al., 2015). Then, the CO desorption experiences a noteworthy increase at higher temperatures, being associated with weak acidic groups, like phenol (600–700 °C), and especially to neutral or basic oxygenated functional groups: carbonyl (700–980 °C), ethers (700 °C) and quinones (700–980 °C) (Shafeeyan et al., 2010; Shen et al., 2012). In summary, the intensity of the CO desorption peak in both MSP700-derived materials, especially at temperatures >700 °C, denotes the presence of a higher proportion of oxygenated groups with basic nature, particularly higher in case of the steam activated sample (Ghouma et al., 2018). In

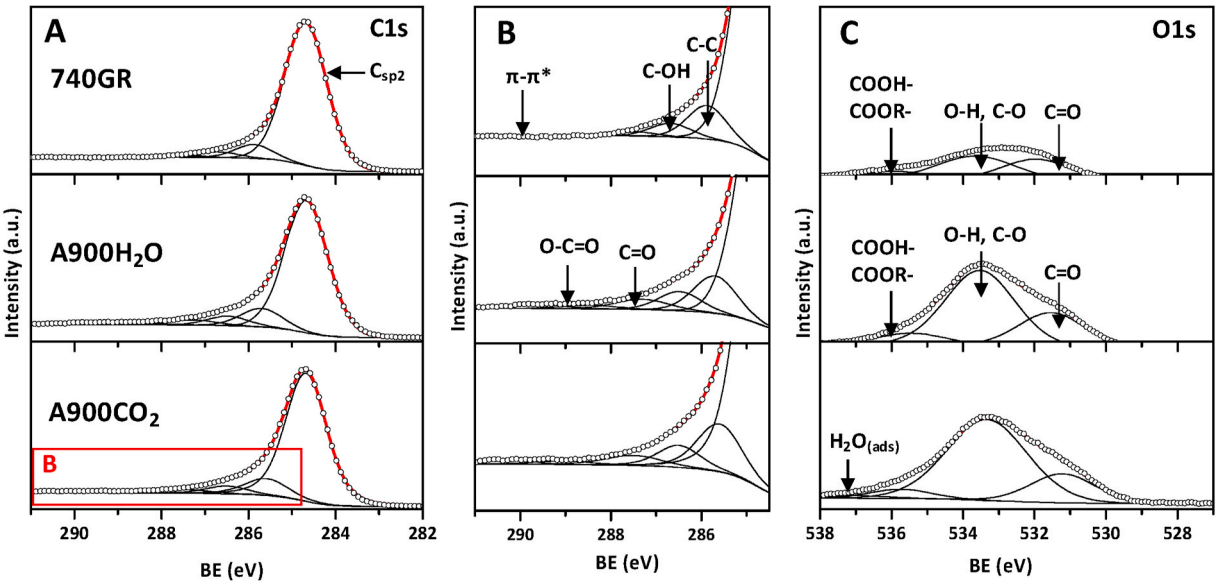

Fig. 4. High-resolution XPS spectra of C1s (A–B) and O1s (C) regions for 740GR, A900CO_2 and A900H_2O.

contrast, for the 740GR active carbon, all the desorbed gases present a much lower intensity than those of MSP700-derived materials, especially H_2O and CO_2 signals; only a peak above 600 °C corresponding to the release of CO is clearly observed, which could be assigned to phenols and, mainly to carbonyl and/or quinone basic groups.

These results indicate that the commercial activated carbon sample possesses mainly basic or neutral functional oxygenated groups, but in a much lower proportion than in the MSP700 activated biochars, which agrees well with the pH_{PZC} measurements of 9.5, 9.9 and 10.1 for 740GR, A900CO_2 and A900H_2O, respectively. These last samples also exhibit certain acidity, which agrees well with the previous observations derived from XPS and TPD-MS analyses.

3.2. NO removal activity tests from polluted gaseous streams

Once the MPS700-derived activated biochars and the 740GR commercial active carbon were physico-chemically characterized, they were tested on the NO elimination at low concentration (5 ppm) from different gaseous streams.

3.2.1. Breakthrough curves and total NO removal capacity of activated biochars

To evaluate the ability of the NO removal of the different CO_2 and H_2O activated biochars, NO breakthrough curves were determined at room temperature under air and N_2 flows (Fig. 6A). These experiments were compared to those attained over the commercial carbon 740GR. In general, all the materials show worse NO removal ability in nitrogen than in air flow, denoting that the presence of oxygen is a critical aspect for an effective NO elimination by biochars-derived carbons, in accordance with literature (Zeng et al., 2012). In this regard, when oxygen gas is present, both physical and chemical adsorption of NO are significantly enhanced (Zhang et al., 2008). This finding is attributed to the fact that, although NO_2 is not detected in the outlet stream, the NO removal at low concentrations predominately occurs via NO oxidation by co-adsorbed O_2 on the carbon surface forming NO_2, that is more easily adsorbed by activated carbons as shown by Xu et al. (2003). This fact is related to the different adsorption energies of NO and NO_2. Thus, Zhu et al. estimated that the adsorption energy for the NO_2 chemisorption in the two possible configurations: N-down (−272.1 kJ/mol) or OO-down (−395.0 kJ/mol) (Zhu et al., 2019), resulted significantly more negative than in case of NO chemisorption, in its two likely configurations: N-down (−225.3 kJ/mol) or O-down (−96.8 kJ/mol) (Zhu et al., 2022), which would imply that NO_2 is more readily adsorbed by the activated carbon. The CO_2-activated biochars exhibit a very low NO removal efficiency in nitrogen flow, achieving C/C_0 values in the range of 0.72–0.87 at a time of 30 min. The efficiency barely increases with the activation temperature reaching a maximum of 16.5% NO removal for the A900CO_2 sample after 400 min. The improved NO elimination capacity with higher activation temperatures may be ascribed either to a higher surface areas achieved or enhanced accessibility of acidic NO to a more basic oxygen functionalities on carbon surface, which may assist the NO adsorption when oxygen gas is absent (Ghafari et al., 2019; Zeng et al., 2012). This increase in the surface basicity is evidenced by the increase in their pH_{PZC} values from 7.5 > 8.2 > 9.9 for samples activated at 800, 850 and 900 °C, respectively, which agrees well with the literature (Sutrisno and Hidayat, 2015). In line with this finding, earlier works have concluded that NO practically is not adsorbed at room temperature in the absence of oxygen, and therefore, only the presence of surface oxygen groups on carbon might assist the NO adsorption in some extension (Zeng et al., 2012; Zhang et al., 2008). On the other hand, the H_2O-activated biochar behaved somewhat better than the CO_2-activated samples, achieving a C/C_0 value of 0.36 after 30 min of the experiment, and a total NO removal of 26.6% at the end of the assay. The better performance of the steam-activated sample in the absence of oxygen, compared to the CO_2-activated one, may be originated by its slightly more basic surface (i.e. pH_{PZC} of 10.1 vs. 9.9) than to its textural properties, which are rather similar (Table 2). The commercial carbon (740GR) exhibits better performance in these conditions, showing a full NO removal during the first 30 min of the test and a breakthrough time close to 50 min, which can be associated with its higher surface area.

In air flow, the breakthrough curve of the commercial carbon (740GR) displays a complete NO removal for the first 60 min of the experiment. At this point, this material begins to be saturated, reducing the NO removal efficiency until C/C_0 values of 0.56. Interestingly, the CO_2-activated biochars, which possess much lower values of S_{BET} and S_{MICRO}, exhibited a higher NO removal efficiency showing values of C/C_0 <0.05 during the whole experiment. Steam-activated biochar behaved similarly to the CO_2-activated material with a practically flat C/C_0 profile, removing almost all NO since the beginning of the test. In this sense, the total NO removal capacity (during the 400 min of the assay) of MSP700-derived materials and commercial active carbon (740GR) was plotted against the materials' BET surface area in Fig. 6B.

In air flow, all MSP700-activated biochars reached an almost total NO removal, with elimination percentages ranging from 97.8 to 99.9%,

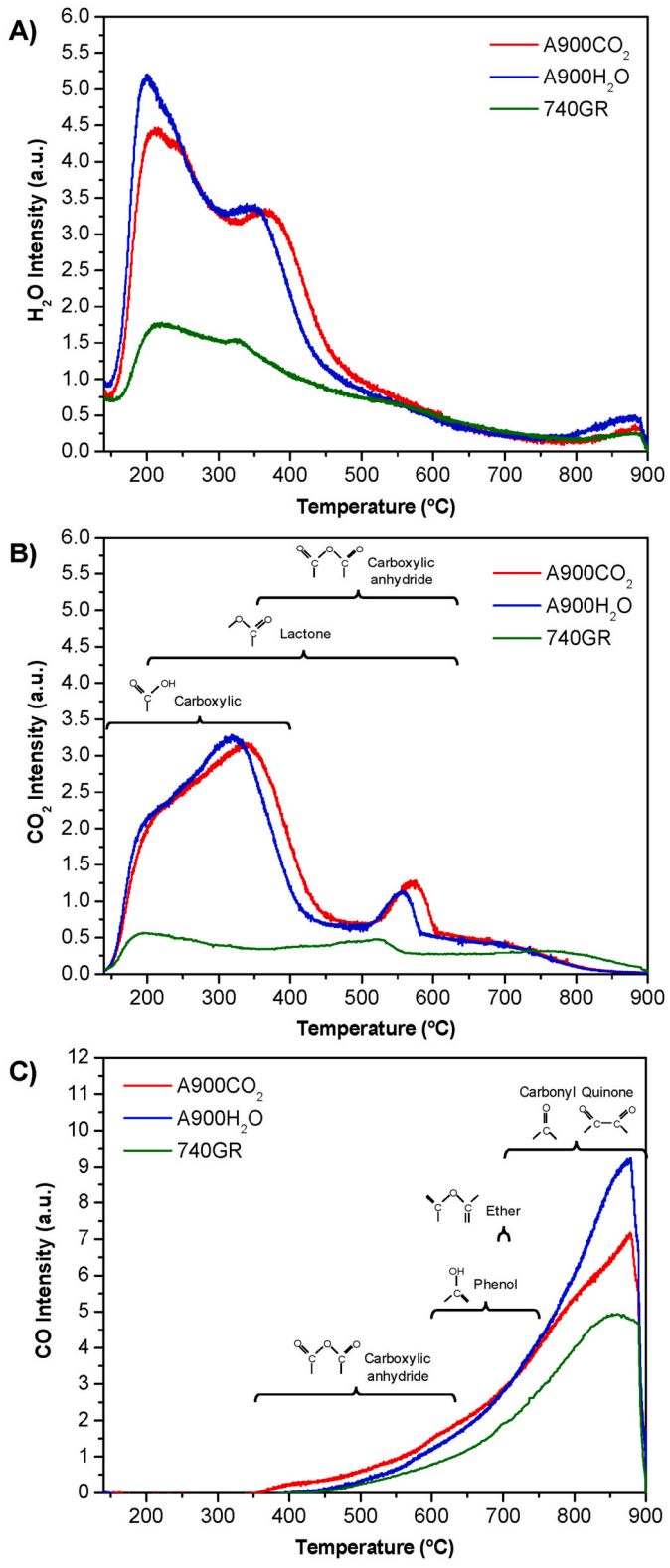

Fig. 5. H_2O, CO_2 and CO TPD-MS spectra of MSP700-derived and commercial (740GR) activated carbons.

which are much higher than that of the commercial carbon (72.6%) despite their lower specific surface area (see Table 2). These results reveal that the surface area of the activated carbons is not the major determining feature for the NO removal at low concentrations in the presence of oxygen. The absence of a clear correlation between NO removal and surface area has been also observed in previous studies devoted to the elimination of NO from flue gases with higher NOx contents (>100 ppm) (Abdulrasheed et al., 2018; Belala et al., 2014; Zhang et al., 2008). On the contrary, Zhang et al. suggested that the conversion of NO into NO_2 in narrow micropores has a strong dependence on the micropore size (with an optimal value on 7 Å) (Zhang et al., 2008; Zhang et al., 2014b). This agrees well with the excellent NO removal capacity of MSP700 activated biochars, which possess a narrow micropore size distribution centred at 6 Å. Therefore, from the kinetic diameters of O_2 and NO are 3.46 and 3.17 Å, respectively, can be envisaged that O_2 and NO molecules are co-adsorbed in these narrow micropores, they will have to contact very closely each other, thus acting as nanoreactors for NO oxidation over surface active sites.

In this regard, the lower ability of 740GR for NO removal could be related to its broad micropore size distribution, with pore diameters ranging from 6 to 17 Å, as well as the lower concentration of surface oxygen groups that may also assist the NO conversion, acting as adsorption sites of NO and O_2 (Shen et al., 2016).

3.2.2. *Effect of the oxygen concentration on the NO removal capacity from gas stream*

Since the presence of O_2 in the gas atmosphere seems to have a strong influence on the NO elimination capacity of carbonaceous materials, a more detailed study was performed increasing the oxygen concentration in the gas stream from 0 to 4, 15 and 21 vol% (air flow). The total flow rate and NO concentration were preserved at 1000 Nml/min and 5 ppm NO, respectively. This study was performed with the $A900CO_2$ and the commercial active carbon 740GR. Fig. 7A displays the effect of the oxygen concentration on the breakthrough curves of NO elimination for 740GR. As can be seen, in the absence of oxygen, the NO concentration at the outlet of the adsorption bed almost reached the value of the feed ($C/C_0 = 0.9$) after 150 min of the experiment. However, the introduction of a low concentration of oxygen in the atmosphere (4 vol%) notably shifted the breakthrough curve to nearly half value ($C/C_0 = 0.47$) at the same time of the experiment. Increasing oxygen concentrations further decreased the C/C_0 although at a lower rate, as shown in Fig. 7B, where the total NO elimination for 400 min of adsorption test is represented as a function of the oxygen concentration in the gas flow. It seems that the nature of the activated carbon precursor, mineral (740GR) or lignocellulosic (MSP700-derived), determine their textural and chemical properties, which plays an important role in the NO removal process. As occurred in the reported literature, the correlation of the NO oxidation with the increase of oxygen concentration is not obvious and depend on the nature of the activated carbon precursor (Guo et al., 2001; Zhang et al., 2008). In this regard, it can be appreciated that in the case of 740GR, there is a clear enhancement of the NO removal as oxygen concentration is increased up to 15 vol%, while its capacity barely raised from 71.1 to 72.6% increasing oxygen up to the air content. This finding suggests that in the case of the commercial carbon, increasing oxygen in the gas phase facilitates its adsorption on the carbon surface generating more C(O) active sites that promote the NO adsorption. However, in the case of $A900CO_2$, its capacity increased from 16.6% to more than 99.9% upon introduction of just 4 vol% O_2 in the gas stream and no further changes were observed with the oxygen concentration. These results reveal that if just a small amount of O_2 is present, the NO removal capacity of this material is strongly improved, confirming that, the removal of NO at low concentrations is governed by NO oxidation to NO_2, as earlier described in the literature for gas streams with high NO contents (Adapa et al., 2006; Kong and Cha, 1996; Shen et al., 2016; Tsukahara et al., 1999). Thus, in the absence of oxygen, the NO removal seems to be more controlled by a physical adsorption, although the presence of basic surface functionalities may partially assist the NO oxidation.

In the case of $A900CO_2$, low concentration of oxygen (4 vol%) is required to achieve almost full elimination of NO, which can be related to the larger amount of oxygen surface functionalities (as shown in TPD-MS and XPS analyses) and a narrower PSD with an average pore size

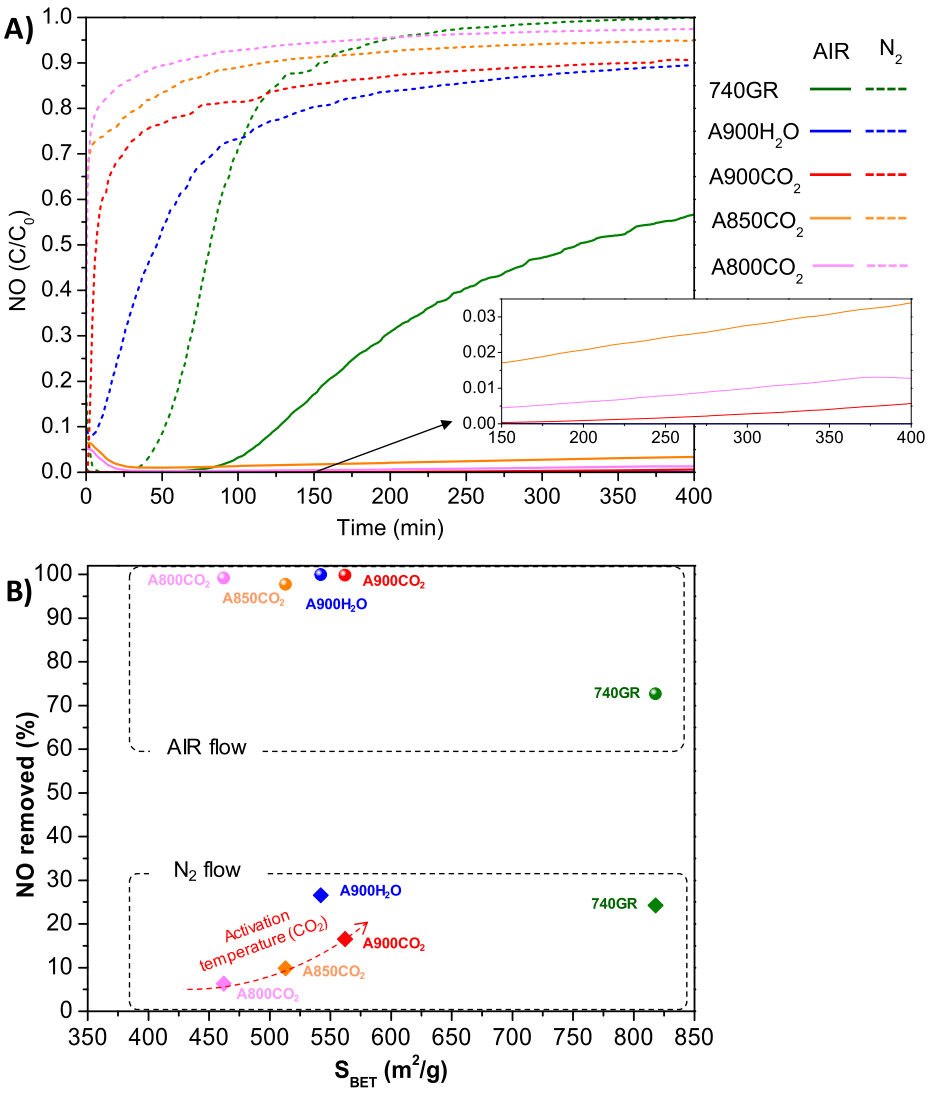

Fig. 6. (A) Breakthrough curves of NO removal of CO_2-activated (800, 850, 900 °C), H_2O-activated (900 °C) biochars and commercial active carbon (740GR); magnification (150–400 min) for MSP700 activated biochars in air (inset); and (B) NO removal capacity of CO_2 and H_2O activated MSP700 biochars and commercial active carbon (740GR) vs specific surface area. Gas flow: dry air (circles) and dry N_2 (diamonds). Total flow rate: 1000 NmL/min; C_0 of NO = 5 ppm; temperature: 20 °C; time: 400 min.

close to 6 Å, in comparison with 740GR, which favor the co-adsorption of NO/O_2 and the further oxidation of NO into NO_2.

3.2.3. *Effect of temperature on the NO removal capacity from gas streams*

The influence of the test temperature (20, 50 and 75 °C) on the adsorption performance of the MSP700-activated biochar ($A900CO_2$) and commercial active carbon 740GR was also investigated and is shown in Fig. 8.

In this case, the total flow rate (air or N_2) and the NO concentration were maintained at 1000 Nml/min and 5 ppm NO, respectively. From this figure, it can be noticed that the removal capacity of commercial carbon 740GR significantly decreased when increasing the adsorption temperature, both in air and nitrogen flows. This finding suggests that over this sample, the physical adsorption of reactants and, in particular NO physisorption, is the limiting stage for the NO removal process. Similar observations have been reported in the literature (Guo et al., 2001; Klose and Rincón, 2007; Zhao et al., 2016b). Thus, Zhao et al. observed that the reaction temperature decreased the NO adsorption capacity of two molecularly imprinted adsorbents, due to the exothermic reactions between NO and the adsorbent, further verifying that the adsorption of NO was a weak physical-sorption interaction easily affected by temperature (Zhao et al., 2016b). Similarly, Klose and Rincón found that the breakthrough times became shorter with increasing temperatures over a coal activated sample (Klose and Rincón, 2007).

In contrast, in this work, the NO elimination under air flow and using physically activated MSP700 biochar was barely altered with temperature, displaying an almost full NO removal during the whole experiment (99–100%). Such results suggest that in this case the NO removal is not governed by a simple physical adsorption mechanism on the micropores, confirming the important role of the chemisorption of both species, NO and O_2 on carbon active sites. Moreover, in the absence of oxygen, MSP700-derived carbon exhibited an increasing capacity favored with temperature that could be related to a higher interaction of NO with active oxygenated surface groups (C(O)). This fact confirms that, in case of biochar-derived samples, the limiting step of the NO removal process would be of chemical nature, as physical adsorption is unfavored by increased temperature.

In conclusion, herein is demonstrated that MSP700-derived carbon could satisfactorily operate in air at any temperature (20–75 °C) not evidencing any signal of deactivation/saturation after 400 min of utilisation; whilst the performance of the commercial carbon (740GR) importantly decays with temperature due to it is controlled by a physical adsorption process, which would imply its reduced adequacy in a real biofilter application.

3.2.4. *Humidity effect*

Humidity plays a very important role in the oxidative conversion of

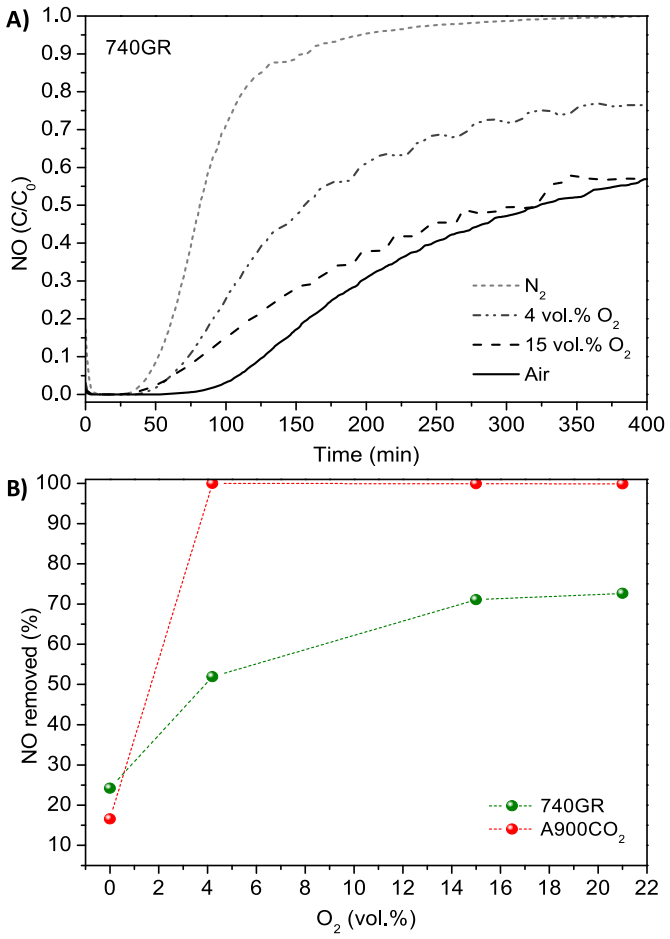

Fig. 7. Effect of the gas stream O_2 concentration on the NO removal breakthrough curves of 740GR (A); and on the total NO removed by 740GR and A900CO_2 (B). Experimental conditions: total flow rate: 1000 NmL/min; NO (C_0 = 5 ppm); temperature: 20 °C; time: 400 min.

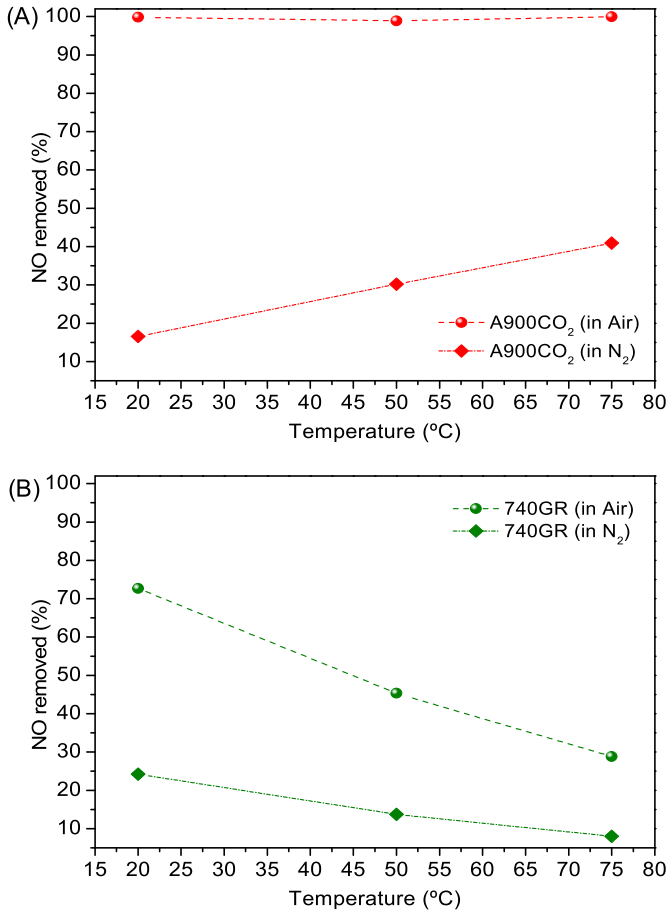

Fig. 8. Effect of the temperature on the total NO removal capacity from dry gas (N_2 or air) flow of CO_2 activated biochar derived from MSP700 and the commercial active carbon (740GR). N_2 (diamond), air (circle). Experimental conditions: total flow rate: 1000 NmL/min; NO (C_0 = 5 ppm); time: 400 min.

NO since polluted air in confined places may contain certain moisture, inherent to the ambient conditions and fuel combustion. Therefore, the effect of the presence of humidity in the air flow (50 vol% RH) during the NO removal tests was evaluated for the MSP700 activated materials (A900CO_2 and A900H_2O) compared with the performance of the commercial active carbon (740GR). The breakthrough curves in both dry and humid air streams are depicted in Fig. 9. In this case, the total flow rate of air and NO concentration were maintained at 1000 Nml/min and 5 ppm of NO, respectively.

Here, activated MSP700 biochars behaved similarly under humid air, showing rather parallel curves as previously observed under dry air flow conditions and, while they exhibited some deactivation as shown by the increasing C/C_0 slope from 100 min, the final value hardly reached 0.1 after 400 min test. This observation denoted that the presence of H_2O, although detrimental for the NO adsorption and subsequent oxidation, did not severely affect the total removal capacity of MSP700-derived carbons, which was still higher than 96%, in good agreement with previous literature (Ghafari and Atkinson, 2016; Klose and Rincón, 2007; Kong and Cha, 1996). In contrast, the commercial active carbon (740GR) showed a much faster deactivation in presence of humidity with a continuous increase of C/C_0 up to 0.5, and a total removal capacity of barely 61.5%, which could be related to the lower proportion of oxygenated surface groups, which are more rapidly inhibited by water molecules. These findings correlate well with previous literature that reported the competition of water molecules and NO/O_2 for the adsorption sites (Kong and Cha, 1996). Wang et al. also estimated by DFT calculations the stronger affinity of H_2O than O_2 in a carbon

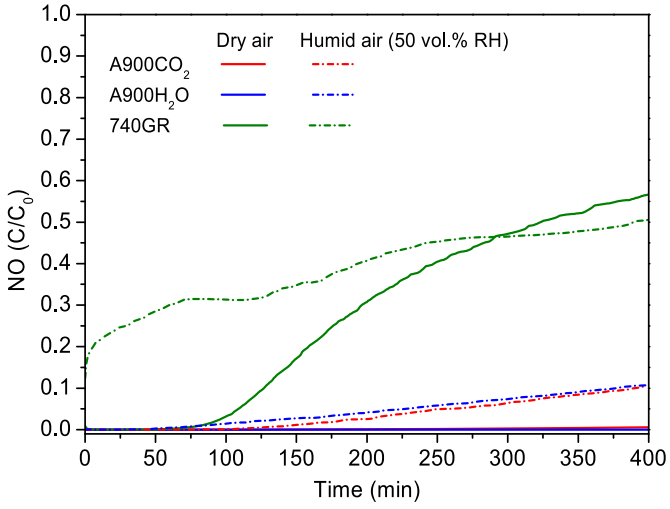

Fig. 9. Effect of the relative humidity (50 vol% HR) in the air flow on the breakthrough curves for the NO removal of MSP700 activated biochars and commercial active carbon (740GR). Total flow rate: 1000 NmL/min. Temperature: 20 °C; NO (C_0 = 5 ppm).

nanotubes (CNTs) sample, due to its large dipolar moment (Wang et al., 2021).

4. Conclusions

In this study, we investigated the performance of several Miscanthus biochar-derived carbons in the removal of NO at low concentration (5 ppm). The effect of the gas stream composition (i.e. the oxygen concentration and relative humidity), and temperature (20–75 °C) have been evaluated and compared against the performance of a commercial carbon (740GR). In this case, 740GR showed a strong dependency on the oxygen concentration and temperature, showing a maximum capacity of 72.6% in air at 20 °C. The presence of H_2O in the air stream lowered its NO removal performance by 15% at 20 °C as it competes with O_2 for surface active sites. This removal capacity markedly decreased with temperature, revealing that physical NO adsorption is the limiting step for the commercial sample, which is related to its initial limited content of oxygen surface functionalities. In contrast, the MSP700-activated biochars (A900CO_2 and A900H_2O) reached a full NO removal (99.9%) at any temperature in air flow, and they needed a low concentration of oxygen (4 vol%) in the gas to achieve full NO removal at 20 °C. Besides, they still showed an excellent performance in the presence of H_2O, with a NO removal capacity higher than 96%. This outstanding NO removal capacity of MSP700-activated biochars arises from the combination of several factors. On the one hand, the surface chemistry of carbons, defined by the nature of the starting materials and activation methods, is an important factor determining their performance. MSP700-derived carbons have highly functionalized surfaces, especially rich in basic oxygenated surface groups. These functionalities act as active sites for NO/O_2 co-adsorption and subsequent oxidation of NO to NO_2, which is further retained over the carbon surface. On the other hand, the homogeneous and narrow micropore distribution of MSP700-derived carbons (centred at 6 Å) facilitates an intimate contact between NO and O_2. However, textural properties (BET surface area and pore size distribution) are not considered as controlling factors by themselves for NO adsorption and further oxidation.

This work shows the significant potential of low-cost and renewable activated carbons, derived from lignocellulosic biomass, for the removal of low NO concentrations (<20 ppm) from polluted ambient air in built environment. Although, at this stage of the investigation, we have not done a cost-study yet, it will be considered for future works. This study also opens the door to future investigations on the optimization and parametrization of the activation and NO removal processes, based on in-depth understanding of the underlying reaction mechanism.

Credit author statement

Carlos G. Díaz-Maroto: Methodology, Software, Formal analysis, Investigation, writing, Visualization; Blanca Sáenz de Miera: Investigation; Laura Collado: Writing – review & editing; Jose Fermoso: activated carbon sample, review and editing; Ondřej Mašek: biochar sample, review and editing; Patricia Pizarro: Writing – review & editing, Supervision; David P. Serrano: Writing – review & editing, Supervision; Inés Moreno: Conceptualization, Validation, Writing – review & editing, Supervision; Javier Fermoso: Conceptualization, Methodology, Validation, Writing – original draft, review and editing, Visualization, Supervision, Funding acquisition.

Declaration of competing interest

The authors declare that they have no known competing financial interests or personal relationships that could have appeared to influence the work reported in this paper.

Data availability

Data will be made available on request.

Acknowledgements

J. Fermoso gratefully acknowledges the financial support from the Comunidad de Madrid through the Talent Attraction Programme (2018-T1/AMB-10023).

Appendix A. Supplementary data

Supplementary data to this article can be found online at https://doi.org/10.1016/j.jenvman.2023.117610.

References

Abdulrasheed, A.A., Jalil, A.A., Triwahyono, S., Zaini, M.A.A., Gambo, Y., Ibrahim, M., 2018. Surface modification of activated carbon for adsorption of SO_2 and NOX: a review of existing and emerging technologies. Renew. Sustain. Energy Rev. 94, 1067–1085. https://doi.org/10.1016/j.rser.2018.07.011.

Adapa, S., Gaur, V., Verma, N., 2006. Catalytic oxidation of NO by activated carbon fiber (ACF). Chem. Eng. J. 116, 25–37. https://doi.org/10.1016/j.cej.2005.10.007.

Ahmed, M.B., Zhou, J.L., Ngo, H.H., Guo, W., Chen, M., 2016. Progress in the preparation and application of modified biochar for improved contaminant removal from water and wastewater. Bioresour. Technol. 214, 836–851. https://doi.org/10.1016/j.biortech.2016.05.057.

Barroso-Bogeat, A., Alexandre-Franco, M., Fernández-González, C., Gómez-Serrano, V., 2019. Activated carbon surface chemistry: changes upon impregnation with Al(III), Fe(III) and Zn(II)-metal oxide catalyst precursors from NO3− aqueous solutions. Arab. J. Chem. 12, 3963–3976. https://doi.org/10.1016/j.arabjc.2016.02.018.

Belala, Z., Belhachemi, M., Jeguirim, M., 2014. Activated carbon prepared from date pits for the retention of NO_2 at low temperature. Int. J. Chem. React. Eng. 12, 717–726. https://doi.org/10.1515/ijcre-2014-0043.

Cha, J.S., Park, S.H., Jung, S.C., Ryu, C., Jeon, J.K., Shin, M.C., Park, Y.K., 2016. Production and utilization of biochar: a review. J. Ind. Eng. Chem. 40, 1–15. https://doi.org/10.1016/j.jiec.2016.06.002.

Chang, C.F., Chang, C.Y., Tsai, W.T., 2000. Effects of burn-off and activation temperature on preparation of activated carbon from corn cob agrowaste by CO_2 and steam. J. Colloid Interface Sci. 232, 45–49. https://doi.org/10.1006/jcis.2000.7171.

Chen, B., Zhou, D., Zhu, L., 2008. Transitional adsorption and partition of nonpolar and polar aromatic contaminants by biochars of pine needles with different pyrolytic temperatures. Environ. Sci. Technol. 42, 5137–5143. https://doi.org/10.1021/es8002684.

Chen, Y., Zhang, X., Chen, W., Yang, H., Chen, H., 2017. The structure evolution of biochar from biomass pyrolysis and its correlation with gas pollutant adsorption performance. Bioresour. Technol. 246, 101–109. https://doi.org/10.1016/j.biortech.2017.08.138.

Chun, Y., Sheng, G., Chiou, G.T., Xing, B., 2004. Compositions and sorptive properties of crop residue-derived chars. Environ. Sci. Technol. 38, 4649–4655. https://doi.org/10.1021/es035034w.

Degrauewe, B., Pisoni, E., Peduzzi, E., de Meij, A., Monforti-Ferrario, F., Bodis, K., Mascherpa, A., Astorga-Llorens, M., Thunis, P., Vignati, E., 2019. Urban NO_2 Atlas. https://doi.org/10.2760/43523.

Delmotte, L., Dufour, A., Elmay, Y., Brosse, N., Gadiou, R., Brech, Y. Le, 2015. Characterization of Miscanthus pyrolysis by DRIFTs, UV Raman spectroscopy and mass spectrometry. J. Anal. Appl. Pyrolysis 113, 402–411. https://doi.org/10.1016/j.jaap.2015.03.004.

Deng, W., Tao, C., Cobb, K., Zhou, H., Su, Y., Ruan, R., 2020. Catalytic oxidation of NO at ambient temperature over the chars from pyrolysis of sewage sludge. Chemosphere 251, 126429. https://doi.org/10.1016/j.chemosphere.2020.126429.

Derwent, R., Hjellbrekke, A.-G., 2019. Air Pollution by Ozone across Europe: Handbook of Environmental Chemistry. EEA Report No 4/2012.

Figueiredo, J.L., Pereira, M.F.R., 2010. The role of surface chemistry in catalysis with carbons. Catal. Today 150, 2–7. https://doi.org/10.1016/j.cattod.2009.04.010.

Figueiredo, J.L., Pereira, M.F.R., Freitas, M.M.A., Órfão, J.J.M., 1999. Modification of the surface chemistry of activated carbons. Carbon N. Y. 37, 1379–1389. https://doi.org/10.1016/S0008-6223(98)00333-9.

Fritz, O.W., Ttinger, K.J.H., 1993. Active sites and intrinsic rates of carbon-gas reactions. A definite confirmation with the carbon-carbon dioxide reaction. Carbon N. Y. 31, 923–930.

Garrido, J., Linares-Solano, A., Martin-Martinez, J.M., Molina-Sabio, M., Rodriguez-Reinoso, F., Torregrosa, R., 1987. Use of nitrogen vs. carbon dioxide in the characterization of activated carbons. Langmuir 3, 76–81. https://doi.org/10.1021/la00073a013.

Ghafari, M., Atkinson, J.D., 2016. Catalytic NO oxidation in the presence of moisture using porous polymers and activated carbon. Environ. Sci. Technol. 50, 5189–5196. https://doi.org/10.1021/acs.est.5b05443.

Ghafari, M., Ghamkhar, R., Atkinson, J.D., 2019. NO oxidation in dry and humid conditions using hyper-cross-linked polymers: impact of surface chemistry on

catalytic conversion efficiency. Fuel 241, 564–570. https://doi.org/10.1016/j.fuel.2018.12.050.
Ghouma, I., Jeguirim, M., Dorge, S., Limousy, L., Matei Ghimbeu, C., Ouederni, A., 2015. Activated carbon prepared by physical activation of olive stones for the removal of NO_2 at ambient temperature. Compt. Rendus Chem. 18, 63–74. https://doi.org/10.1016/j.crci.2014.05.006.
Ghouma, I., Jeguirim, M., Sager, U., Limousy, L., Bennici, S., Däuber, E., Asbach, C., Ligotski, R., Schmidt, F., Ouederni, A., 2017. The potential of activated carbon made of agro-industrial residues in NOx immissions abatement. Energies 10, 1508. https://doi.org/10.3390/en10101508.
Ghouma, I., Jeguirim, M., Limousy, L., Bader, N., Ouederni, A., Bennici, S., 2018. Factors influencing NO_2 adsorption/reduction on microporous activated carbon: porosity vs. surface chemistry. Materials 11. https://doi.org/10.3390/ma11040622.
González, J.F., Román, S., González-García, C.M., Nabais, J.M.V., Ortiz, A.L., 2009. Porosity development in activated carbons prepared from walnut shells by carbon dioxide or steam activation. Ind. Eng. Chem. Res. 48, 7474–7481. https://doi.org/10.1021/ie9013293.
Guo, Z., Xie, Y., Hong, I., Kim, J., 2001. Catalytic oxidation of NO to NO_2 on activated carbon. Energy Convers. Manag. 42, 2005–2018. https://doi.org/10.1016/S0196-8904(01)00058-9.
Haerle, R., Riedo, E., Pasquarello, A., Baldereschi, A., 2002. sp2/sp3 hybridization ratio in amorphous carbon from C 1s core-level shifts: X-ray photoelectron spectroscopy and first-principles calculation. Phys. Rev. B Condens. Matter 65, 1–9. https://doi.org/10.1103/PhysRevB.65.045101.
Hodjati, S., Vaezzadeh, K., Petit, C., Pitchon, V., Kiennemann, A., 2000. Absorption/desorption of NOx process on perovskites: performances to remove NOx from a lean exhaust gas. Appl. Catal. B Environ. 26, 5–16. https://doi.org/10.1016/S0926-3373(99)00143-5.
Huang, Y., Liu, Y., Zhao, G., Chen, J.Y., 2017. Sustainable activated carbon fiber from sawdust by reactivation for high-performance supercapacitors. J. Mater. Sci. 52, 478–488. https://doi.org/10.1007/s10853-016-0347-0.
Hwang, H., Sahin, O., Choi, J.W., 2017. Manufacturing a super-active carbon using fast pyrolysis char from biomass and correlation study on structural features and phenol adsorption. RSC Adv. 7, 42192–42202. https://doi.org/10.1039/c7ra06910c.
Ishii, T., Kyotani, T., 2016. Temperature programmed desorption. In: Materials Science and Engineering of Carbon. Tsinghua University Press Limited, pp. 287–305. https://doi.org/10.1016/b978-0-12-805256-3.00014-3.
Jafri, N., Wong, W.Y., Doshi, V., Yoon, L.W., Cheah, K.H., 2018. A review on production and characterization of biochars for application in direct carbon fuel cells. Process Saf. Environ. Protect. 118, 152–166. https://doi.org/10.1016/j.psep.2018.06.036.
Jagiello, J., Kenvin, J., Celzard, A., Fierro, V., 2019. Enhanced resolution of ultra micropore size determination of biochars and activated carbons by dual gas analysis using N_2 and CO_2 with 2D-NLDFT adsorption models. Carbon N. Y. 144, 206–215. https://doi.org/10.1016/j.carbon.2018.12.028.
Jeguirim, M., Belhachemi, M., Limousy, L., Bennici, S., 2018. Adsorption/reduction of nitrogen dioxide on activated carbons: textural properties versus surface chemistry – a review. Chem. Eng. J. 347, 493–504. https://doi.org/10.1016/j.cej.2018.04.063.
Jiang, H., Zhang, L., Wang, X., Holm, N., Rajagopalan, K., Chen, F., Ma, S., 2013. Highly ordered macroporous woody biochar with ultra-high carbon content as supercapacitor electrodes. Electrochim. Acta 113, 481–489. https://doi.org/10.1016/j.electacta.2013.09.121.
Keiluweit, M., Nico, P.S., Johnson, M., Kleber, M., 2010. Dynamic molecular structure of plant biomass-derived black carbon (biochar). Environ. Sci. Technol. 44, 1247–1253. https://doi.org/10.1021/es9031419.
Klose, W., Rincón, S., 2007. Adsorption and reaction of NO on activated carbon in the presence of oxygen and water vapour. Fuel 86, 203–209. https://doi.org/10.1016/j.fuel.2006.06.017.
Kong, Y., Cha, C.Y., 1996. NOx adsorption on char in presence of oxygen and moisture. Carbon N. Y. 34, 1027–1033. https://doi.org/10.1016/0008-6223(96)00050-4.
Labaki, M., Issa, M., Smeekens, S., Heylen, S., Kirschhock, C.E.A., Villani, K., Jeguirim, M., Habermacher, D., Brilhac, J.F., Martens, J.A., 2010. Modeling of NOx adsorption-desorption-reduction cycles on a ruthenium loaded Na-Y zeolite. Appl. Catal. B Environ. 97, 13–20. https://doi.org/10.1016/j.apcatb.2010.03.002.
Levasseur, B., Ebrahim, A.M., Burress, J., Bandosz, T.J., 2011. Interactions of NO_2 at ambient temperature with cerium-zirconium mixed oxides supported on SBA-15. J. Hazard Mater. 197, 294–303. https://doi.org/10.1016/j.jhazmat.2011.09.087.
Li, H., Dong, X., da Silva, E.B., de Oliveira, L.M., Chen, Y., Ma, L.Q., 2017. Mechanisms of metal sorption by biochars: biochar characteristics and modifications. Chemosphere 178, 466–478. https://doi.org/10.1016/j.chemosphere.2017.03.072.
Liu, W.J., Jiang, H., Yu, H.Q., 2015. Development of biochar-based functional materials: toward a sustainable platform carbon. Material. Chem. Rev. 115, 12251–12285. https://doi.org/10.1021/acs.chemrev.5b00195.
Mašek, O., Buss, W., Roy-Poirier, A., Lowe, W., Peters, C., Brownsort, P., Mignard, D., Pritchard, C., Sohi, S., 2018. Consistency of biochar properties over time and production scales: a characterisation of standard materials. J. Anal. Appl. Pyrolysis 132, 200–210. https://doi.org/10.1016/j.jaap.2018.02.020.
Mimmo, T., Panzacchi, P., Baratieri, M., Davies, C.A., Tonon, G., 2014. Effect of pyrolysis temperature on miscanthus (Miscanthus × giganteus) biochar physical, chemical and functional properties. Biomass Bioenergy 62, 149–157. https://doi.org/10.1016/j.biombioe.2014.01.004.
Mochida, I., Kawabuchi, Y., Kawano, S., Matsumura, Y., Yoshikawa, M., 1997. High catalytic activity of pitch-based activated carbon fibres of moderate surface area for oxidation of NO to NO_2 at room temperature. Fuel 76, 543–548. https://doi.org/10.1016/S0016-2361(96)00223-2.
Mochida, I., Shirahama, N., Kawano, S., Korai, Y., Yasutake, A., Tanoura, M., Fujii, S., Yoshikawa, M., 2000. NO oxidation over activated carbon fiber (ACF). Part 1 . Extended kinetics over a pitch based ACF of very large surface area. Fuel 79, 1713–1723.
Muñiz, J., Marbán, G., Fuertes, A.B., 1999. Low temperature selective catalytic reduction of NO over polyarylamide-based carbon fibres. Appl. Catal. B Environ. 23, 25–35.
Nowicki, P., Pietrzak, R., Wachowska, H., 2010. Sorption properties of active carbons obtained from walnut shells by chemical and physical activation. Catal. Today 150, 107–114. https://doi.org/10.1016/j.cattod.2009.11.009.
Otake, Y., Jenkins, R.G., 1993. Characterization of oxygen-containing surface complexes created on a microporous carbon by air and nitric acid treatment. Carbon N. Y. 31, 109–121. https://doi.org/10.1016/0008-6223(93)90163-5.
Pevida, C., Plaza, M.G., Arias, B., Fermoso, J., Rubiera, F., Pis, J.J., 2008. Surface modification of activated carbons for CO_2 capture. Appl. Surf. Sci. 254, 7165–7172. https://doi.org/10.1016/j.apsusc.2008.05.239.
Qi, G., Pan, Z., Zhang, X., Miao, X., Xiang, W., Gao, B., 2022. Effect of ball milling with hydrogen peroxide or ammonia hydroxide on sorption performance of volatile organic compounds by biochar from different pyrolysis temperatures. Chem. Eng. J. 450, 138027 https://doi.org/10.1016/j.cej.2022.138027.
Qu, J., Wang, Y., Tian, X., Jiang, Z., Deng, F., Tao, Y., Jiang, Q., Wang, L., Zhang, Y., 2021. KOH-activated porous biochar with high specific surface area for adsorptive removal of chromium (VI) and naphthalene from water: affecting factors, mechanisms and reusability exploration. J. Hazard Mater. 401, 123292 https://doi.org/10.1016/j.jhazmat.2020.123292.
Rathore, R.S., Srivastava, D.K., Agarwal, A.K., Verma, N., 2010. Development of surface functionalized activated carbon fiber for control of NO and particulate matter. J. Hazard Mater. 173, 211–222. https://doi.org/10.1016/j.jhazmat.2009.08.071.
Román, S., González, J.F., González-García, C.M., Zamora, F., 2008. Control of pore development during CO_2 and steam activation of olive stones. Fuel Process. Technol. 89, 715–720. https://doi.org/10.1016/j.fuproc.2007.12.015.
Sajjadi, B., Chen, W.Y., Egiebor, N.O., 2019. A comprehensive review on physical activation of biochar for energy and environmental applications. Rev. Chem. Eng. 35, 735–776. https://doi.org/10.1515/revce-2017-0113.
Shafeeyan, M.S., Daud, W.M.A.W., Houshmand, A., Shamiri, A., 2010. A review on surface modification of activated carbon for carbon dioxide adsorption. J. Anal. Appl. Pyrolysis 89, 143–151. https://doi.org/10.1016/j.jaap.2010.07.006.
Shen, W., Li, Z., Liu, Y., 2012. Surface chemical functional groups modification of porous carbon. Recent Pat. Chem. Eng. 1, 27–40. https://doi.org/10.2174/2211334710801010027.
Shen, Y., Ge, X., Chen, M., 2016. Catalytic oxidation of nitric oxide (NO) with carbonaceous materials. RSC Adv. 6, 8469–8482. https://doi.org/10.1039/c5ra24148k.
Sousa, J.P.S., Pereira, M.F.R., Figueiredo, J.L., 2011. Catalytic oxidation of NO to NO_2 on N-doped activated carbons. Catal. Today 176, 383–387. https://doi.org/10.1016/j.cattod.2010.11.040.
Sousa, J.P.S., Pereira, M.F.R., Figueiredo, J.L., 2012. NO oxidation over nitrogen doped carbon xerogels. Appl. Catal. B Environ. 125, 398–408. https://doi.org/10.1016/j.apcatb.2012.06.009.
Sousa, J.P.S., Pereira, M.F.R., Figueiredo, J.L., 2013. Modified activated carbon as catalyst for NO oxidation. Fuel Process. Technol. 106, 727–733. https://doi.org/10.1016/j.fuproc.2012.10.008.
Sutrisno, B., Hidayat, A., 2015. The effects of activation temperature on physico-chemical characteristics of activated carbons derived from biomass wastes. AIP Conf. Proc. 1699 https://doi.org/10.1063/1.4938370.
Sysoev, V.I., Okotrub, A.V., Gusel'nikov, A.V., Smirnov, D.A., Bulusheva, L.G., 2018. In situ XPS observation of selective NOx adsorption on the oxygenated graphene films. Phys. Status Solidi Basic Res. 255 https://doi.org/10.1002/pssb.201700267.
Tan, X., Liu, S., Liu, Y., Gu, Y., Zeng, G., Hu, X., Wang, X., Liu, S., Jiang, L., 2017. Biochar as potential sustainable precursors for activated carbon production: multiple applications in environmental protection and energy storage. Bioresour. Technol. 227, 359–372. https://doi.org/10.1016/j.biortech.2016.12.083.
Thommes, M., Kaneko, K., Neimark, A.V., Olivier, J.P., Rodriguez-Reinoso, F., Rouquerol, J., Sing, K.S.W., 2015. Physisorption of gases, with special reference to the evaluation of surface area and pore size distribution (IUPAC Technical Report). Pure Appl. Chem. 87, 1051–1069. https://doi.org/10.1515/pac-2014-1117.
Tsukahara, H., Ishida, T., Mayumi, M., 1999. Gas-phase oxidation of nitric oxide: chemical kinetics and rate constant. Nitric Oxide - Biol. Chem. 3, 191–198. https://doi.org/10.1006/niox.1999.0232.
Wang, J., Wang, S., 2019. Preparation, modification and environmental application of biochar: a review. J. Clean. Prod. 227, 1002–1022. https://doi.org/10.1016/j.jclepro.2019.04.282.
Wang, M.X., Huang, Z.H., Shimohara, T., Kang, F., Liang, K., 2011. NO removal by electrospun porous carbon nanofibers at room temperature. Chem. Eng. J. 170, 505–511. https://doi.org/10.1016/j.cej.2011.01.017.
Wang, J., Zhu, J., Zhou, X., Du, Y., Huang, W., Liu, J., Zhang, W., Shi, J., Chen, H., 2015. Nanoflower-like weak crystallization manganese oxide for efficient removal of low-concentration NO at room temperature. J. Mater. Chem. 3, 7631–7638. https://doi.org/10.1039/c5ta00468c.
Wang, Y., Hu, X., Guo, T., Tian, W., Hao, J., Guo, Q., 2021. The competitive adsorption mechanism of CO_2, H_2O and O_2 on a solid amine adsorbent. Chem. Eng. J. 416, 1–10. https://doi.org/10.1016/j.cej.2021.129007.
(WHO) , W.H.O., n.d. Air pollution [WWW Document]. URL https://www.who.int/news-room/air-pollution.
Xu, X.H., Shi, Y., Liu, S.H., Wang, H.P., Chang, S.G., Fisher, J.W., Pisharody, S., Moran, M., Wignarajah, K., 2003. Method for the control of NOx emissions in long-range space travel. Energy Fuel. 17, 1303–1310. https://doi.org/10.1021/ef0300803.

Yadav, D., Prasad, R., 2016. Low temperature de-NOx technology-a challenge for vehicular exhaust and its remedation: an overview. Procedia Technol 24, 639–644. https://doi.org/10.1016/j.protcy.2016.05.156.

Yang, T., Lua, A.C., 2003. Characteristics of activated carbons prepared from pistachio-nut shells by physical activation. J. Colloid Interface Sci. 267, 408–417. https://doi.org/10.1016/S0021-9797(03)00689-1.

You, F.T., Yu, G.W., Wang, Y., Xing, Z.J., Liu, X.J., Li, J., 2017. Study of nitric oxide catalytic oxidation on manganese oxides-loaded activated carbon at low temperature. Appl. Surf. Sci. 413, 387–397. https://doi.org/10.1016/j.apsusc.2017.04.044.

Zeng, Z., Lu, P., Li, C., Mai, L., Li, Z., Zhang, Y., 2012. Removal of NO by carbonaceous materials at room temperature: a review. Catal. Sci. Technol. 2, 2188–2199. https://doi.org/10.1039/c2cy20183f.

Zhang, W.J., Rabiei, S., Bagreev, A., Zhuang, M.S., Rasouli, F., 2008. Study of NO adsorption on activated carbons. Appl. Catal. B Environ. 83, 63–71. https://doi.org/10.1016/j.apcatb.2008.02.003.

Zhang, Z., Atkinson, J.D., Jiang, B., Rood, M.J., Yan, Z., 2014b. Nitric oxide oxidation catalyzed by microporous activated carbon fiber cloth: an updated reaction mechanism. Appl. Catal. B Environ. 148–149, 573–581. https://doi.org/10.1016/j.apcatb.2013.10.050.

Zhang, X., Cao, L., Xiang, W., Xu, Y., Gao, B., 2022. Preparation and evaluation of fine-tuned micropore biochar by lignin impregnation for CO_2 and VOCs adsorption. Separ. Purif. Technol. 295, 121295 https://doi.org/10.1016/j.seppur.2022.121295.

Zhang, Y.-J., Xing, Z.-J., Duan, Z.-K., Li, M., Wang, Y., 2014a. Effects of steam activation on the pore structure and surface chemistry of activated carbon derived from bamboo waste. Appl. Surf. Sci. 315, 279–286. https://doi.org/10.1016/j.apsusc.2014.07.126.

Zhao, Y., Wang, H., Wang, T., 2016b. Adsorption of NO from flue gas by molecularly imprinted adsorbents. Chem. Eng. J. 306, 832–839. https://doi.org/10.1016/j.cej.2016.08.023.

Zhao, J., Xia, Y., Li, M., Li, S., Li, W., Zhang, S., 2016a. A biophysicochemical model for NO removal by the chemical absorption-biological reduction integrated process. Environ. Sci. Technol. 50, 8705–8712. https://doi.org/10.1021/acs.est.6b01414.

Zhu, Z., Liu, Z., Liu, S., Niu, H., 2000. Adsorption and reduction of NO over activated coke at low temperature. Fuel 79, 651–658. https://doi.org/10.1016/S0016-2361(99)00192-1.

Zhu, X., Zhang, L., Zhang, M., Ma, C., 2019. Effect of N-doping on NO_2 adsorption and reduction over activated carbon: an experimental and computational study. Fuel 258, 116109. https://doi.org/10.1016/j.fuel.2019.116109.

Zhu, X., Zhang, L., Wang, T., Li, J., Zhou, X., Ma, C., Dong, Y., 2022. An updated study on NO catalytic oxidation over activated carbon: the effect of pore structure and a dual-site mechanism. Fuel 311, 122627. https://doi.org/10.1016/j.fuel.2021.122627.